19970523 080

SMC-TR-96-07

AEROSPACE REPORT NO.
TR-97(8555)-1

Volume-Based Static Model for Nickel-Hydrogen Cells

20 November 1996

Prepared by

L. H. THALLER
Electronics Technology Center
Technology Operations

Prepared for

SPACE AND MISSILE SYSTEMS CENTER
AIR FORCE MATERIEL COMMAND
2430 E. El Segundo Boulevard
Los Angeles Air Force Base, CA 90245

Engineering and Technology Group

THE AEROSPACE CORPORATION
El Segundo, California

APPROVED FOR PUBLIC RELEASE;
DISTRIBUTION UNLIMITED

This report was submitted by The Aerospace Corporation, El Segundo, CA 90245-4691, under Contract No. F04701-93-C-0094 with the Space and Missile Systems Center, 2430 E. El Segundo Blvd., Los Angeles Air Force Base, CA 90245. It was reviewed and approved for The Aerospace Corporation by R. P. Frueholz, Principal Director, Electronics Technology Center. Col. C. Whited was the project officer for the Mission-Oriented Investigation and Experimentation (MOIE) program.

This report has been reviewed by the Public Affairs Office (PAS) and is releasable to the National Technical Information Service (NTIS). At NTIS, it will be available to the general public, including foreign nationals.

This technical report has been reviewed and is approved for publication. Publication of this report does not constitute Air Force approval of the report's findings or conclusions. It is published only for the exchange and stimulation of ideas.

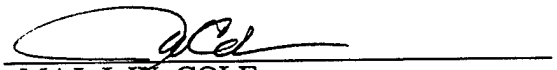

MAJ. J. W. COLE
SMC/AXES

REPORT DOCUMENTATION PAGE

Form Approved
OMB No. 0704-0188

Public reporting burden for this collection of information is estimated to average 1 hour per response, including the time for reviewing instructions, searching existing data sources, gathering and maintaining the data needed, and completing and reviewing the collection of information. Send comments regarding this burden estimate or any other aspect of this collection of information, including suggestions for reducing this burden to Washington Headquarters Services, Directorate for Information Operations and Reports, 1215 Jefferson Davis Highway, Suite 1204, Arlington, VA 22202-4302, and to the Office of Management and Budget, Paperwork Reduction Project (0704-0188), Washington, DC 20503.

1. AGENCY USE ONLY (*Leave blank*)	2. REPORT DATE	3. REPORT TYPE AND DATES COVERED
	20 November 1996	

4. TITLE AND SUBTITLE

Volume-Based Static Model for Nickel-Hydrogen Cells

5. FUNDING NUMBERS

F04701-93-C-0094

6. AUTHOR(S)

L. H. Thaller

7. PERFORMING ORGANIZATION NAME(S) AND ADDRESS(ES)

The Aerospace Corporation
Technology Operations
El Segundo, CA 90245-4691

8. PERFORMING ORGANIZATION REPORT NUMBER

TR-97(8555)-1

9. SPONSORING/MONITORING AGENCY NAME(S) AND ADDRESS(ES)

Space and Missile Systems Center
Air Force Materiel Command
2430 E. El Segundo Boulevard
Los Angeles Air Force Base, CA 90245

10. SPONSORING/MONITORING AGENCY REPORT NUMBER

SMC-TR-96-07

11. SUPPLEMENTARY NOTES

12a. DISTRIBUTION/AVAILABILITY STATEMENT

Approved for public release; distribution unlimited

12b. DISTRIBUTION CODE

13. ABSTRACT (*Maximum 200 words*)

A static nickel-hydrogen cell model has been developed to help explore the long-term performance projections for nickel-hydrogen cells and batteries. The model consists of a spreadsheet arrangement of the volume/porosity/wettability characteristics for each of the cell's wettable components. Following the development of the basic model, the growing databases related to plate expansion, plaque corrosion, and electrolyte management considerations were reviewed as they impact changes in the electrolyte requirements of the cell. The basic model was modified to incorporate these effects. Taken together, the expanded model can be used to project cell performance over the useful life of a particular cell design. The model suggests that an important feature of a cell design is the percentage of the separator's pores that remain filled with electrolyte over the course of cell cycling. Factors that reduce the amount of electrolyte contained in the separator adversely impact the mass transport processes within the cell. This ultimately results in significant performance degradation. These factors include: (1) expansion of the positive plates, (2) corrosion of the nickel sinter substrate material, (3) incorporation of potassium hydroxide (KOH) into the structure of the gamma-phase portion of the charged active material, and (4) condensation of water from the electrolyte onto the colder cell wall. Literature information related to these issues has suggested how materials can be selected, and components can be designed to be better able to accommodate changes in electrolyte volume during the required life of the cell.

14. SUBJECT TERMS

Nickel-hydrogen, Cell Model, Performance projection, Aging effects

15. NUMBER OF PAGES

29

16. PRICE CODE

17. SECURITY CLASSIFICATION OF REPORT	18. SECURITY CLASSIFICATION OF THIS PAGE	19. SECURITY CLASSIFICATION OF ABSTRACT	20. LIMITATION OF ABSTRACT
UNCLASSIFIED	UNCLASSIFIED	UNCLASSIFIED	

Contents

Figures

Tables

1. Introduction

Cycle life testing of nickel-hydrogen cells has produced results that have varied well over an order of magnitude (in terms of cycles to failure) when comparing different cell designs under the same test conditions.[1] Some of the cell designs that were built and tested over a decade ago have shown higher numbers of cycles to deeper depths of discharge compared with cell designs that have been built and tested within the past few years. The actual components in terms of electrodes and separators are very similar in all of these cells, but features of their overall design must have caused the large differences in their cycle lives. A study was initiated in an attempt to discover the reason or reasons behind this wide range of results from seemingly similar cell configurations. The results of this study have suggested guidelines for designs that would circumvent the problems associated with the configurations that have displayed poor cycleability. First, a static model was developed that completely accounts for all the volumetric features of the plate pack within a typical individual pressure vessel (IPV) nickel-hydrogen cell. The model, using a Lotus 1-2-3 format, carefully accounts for the distribution of electrolyte contained within the wettable volumes of the electrodes and separators. This is done by determining all the dimensions, thicknesses, porosities, densities, and wettabilities for the different components within the plate pack along with the amount of electrolyte added to the cell during the activation process. The percentage of wettable volume of each component that is initially filled with electrolyte can then be determined. Capillary forces will tend to distribute the electrolyte between the components in a manner resulting in equal capillary pressures in all the components.[2] Following this, the results of destructive physical analyses from cells of this general type were reviewed. References 3, 4, and 5 present information on the expansion of positive electrodes caused by cycling with different concentrations of KOH, while References 6 and 7 present data on the corrosion rates of the porous nickel sinter substrate. Estimates of the changes in distribution of electrolyte caused by plate expansion and grid corrosion can then be made. With this information on the changes in the electrolyte content of the different cell components as a function of cycling, initial projections can be made for the useful cycle life of different cell designs.

Depending on the details of the cell design, different concentrations and amounts of electrolyte, separator materials, and electrode types are specified. Electrodes, in particular, differ in regard to how they are made. Although they may be similar in dimensions and capacities, they vary according to the process used to manufacture the porous nickel plaque material, the impregnation process used, the type and amount of additive used during the impregnation step, and the amount of active material incorporated into the pores of the sintered nickel substrate. All these factors impact the ultimate cycle life of that design because of the differences in the structural changes that take place within these different nickel electrodes during cycling. Cell designs that have displayed cycle lives in the tens of thousands at deep depths of discharge have been able to accommodate these changes. Provisions for these changes can be designed into a cell if they are fully understood.

Besides the aging phenomenon due to plate expansion and corrosion, there are several other phenomena that alter the condition of the electrolyte within the cell's components. One is related to the extent to which the active material is converted to the gamma phase while the cell is being cycled,

and the other results from the thermal environment imposed on the cell. References 8 and 9 report on the effects of the gamma-phase material and how KOH is incorporated into the lattice structure. This structural phase of the active material is produced during overcharge or within the uncycled active material as some of the beta-phase material gradually transforms into the more thermodynamically stable gamma-phase material. Experimental studies[8] have reported that one third of a mole of KOH is withdrawn from the electrolyte solution and incorporated within the lattice structure of each mole of the gamma phase of nickel oxyhydroxide that is formed. The average valence of nickel ions in the gamma-phase material is 3.66 as opposed to 3.00 in the beta-phase material. A recent publication[10] outlines the impact of the KOH loss from the electrolyte on the diffusion-limiting currents of IPV cells filled with different volumes and starting concentrations of electrolyte. The boundaries for acceptable cell performance as established by diffusional processes of the ionic species within the separator layer were reviewed from several different perspectives. Reference 10 also describes the movement of water vapor under the influence of vapor pressure differences within the cell. Under certain thermal gradients, water can be evaporated from the plate pack and condensed onto a colder cell wall.

The model has been found to be useful in reviewing existing cell designs in terms of the amount of electrolyte used (recorded as grams of solution per ampere hour of cell capacity) or in terms of percent of the wettable pores that are filled with electrolyte. Published and unpublished data associated with a number of different cell designs have shown a definite trend to reduce the amount of electrolyte used in the initial activation and filling steps even though there is ample published evidence that, up to a point, more electrolyte generally provides better cycle life.

2. Factors Impacting the Volumetric Features of Cells

Nickel-hydrogen cells are referred to as being starved. The electrolyte is contained within the capillary structure of the three components of a plate set. In cells using wall wicks,[11] small amounts of electrolyte are contained along its surfaces as well. Wall wicks are wettable surfaces that facilitate the movement of electrolyte within the cell. The majority of the electrolyte is contained within the pore structure of the nickel electrodes, the separators, and the hydrogen electrodes. If it were not for very slow changes in the dimensional aspects of these components, the cycle lives of these cells would only be limited by the structural integrity of the nickel electrode. There are four major factors that cause the cells to slowly fail due to insufficient quantities of electrolyte being contained in the separator. These will be addressed in the following sections.

2.1 Plate Expansion

As nickel electrodes are cycled, they tend to increase in thickness. The rate of expansion has been studied by several investigators and was found to depend on many factors. Lim[5] studied an electrode where the active material and the sinter substrate from one side of the foil current collector had been removed. He was able to detect an expansion as the active material was cycled to deep depths of discharge based on the bending response of the plate. The major portion of the expansion was found to be reversible as the electrode was recharged. However, a small amount of permanent expansion did take place that accumulated over many cycles. Much of the studies of this phenomenon were carried out using electrodes made for nickel-cadmium cells. The amount of active material per unit of void volume was much higher in older nickel-cadmium cells (2.2 g/cm^3 of void volume vs 1.65 g/cm^3 in nickel-hydrogen cells). These higher loading levels permit the expansion characteristics to be seen much earlier compared with electrodes that are less heavily loaded. The work reported by Maurer[3] clearly showed that plate strength, depth of discharge, and number of cycles determined the ultimate thickness of a nickel electrode. Differences were also found between different manufacturing lots of electrodes. Depending on the sintering temperature and the residence time in the sintering furnace, there were differences in the mechanical strength of the unimpregnated sinter. A further cause for variation was related to the amount of corrosion that occurred during the impregnation process. In positive plates made for nickel-hydrogen cells, where deeper depths of discharge and longer cycle lives are desired, greater attention is paid to consistent sinter strength measurements and lighter loading levels of active material. Even within nickel-hydrogen technology, large differences in plate expansion have been experienced.

A significant difference has been attributed to the electrolyte concentration that is added to the cell during the formation process. Lim[12] found that lower electrolyte concentrations resulted in longer cycle lives and lower rates of plate expansion. Higher concentrations of KOH facilitate the conversion of the beta form of the charged material (average valence 3.0) to the gamma phase (average valence 3.66). Higher utilization percentages are also associated with higher amounts of cobalt used as an additive.

The term "utilization" is used to describe the average valance change that takes place as the active material is charged and discharged. It is based on knowing the weight of active material in an electrode and the usable capacity. Then the ratio of these two numbers is taken assuming only one electron is involved in the discharge step. Since the upper limit is 1.66 electrons per mole of active material if all of it were in the gamma phase and if all of the active material were dischargeable, the upper limit for utilization is 166%.

Another factor that leads to plate expansion is related to the weakness of the sinter material of the plaque. Two typical types of plaque materials begin from two very different manufacturing processes. Dry powder sinters are routinely made with a porosity of 84%, which is reduced in a finished plaque to 80% when the nickel screen is factored into the overall porosity. The screen is located near one edge of the plaque and serves as the current collector. Sinter material produced by the slurry process is generally targeted to have a sinter porosity of 80% and a plaque porosity of 76%. This type of plaque material has the screen near the center. It is less porous and has a higher bend strength, but less electrochemical capacity per plate since most modern plates are loaded with 1.6 to 1.7 g/cm^3 void. The thicknesses of finished electrodes center around either 0.030 in. or 0.035 in., although other thicknesses up to 0.080 in. have been reported.[13] Thicker electrodes have lower utilizations of active material at high discharge rates due to the difficulties of being able to maintain good mass transport to the interior of these thicker structures.

For whatever reason and at whatever rate, when plates expand, they tend to draw electrolyte out of the separator by capillary action. The electrolyte will distribute itself in a manner to equilibrate the capillary pressure between communicating components. The separator material usually serves as a reservoir for electrolyte, and due to its larger average pore size, it will give up electrolyte to the positive plate as it expands. A more exact treatment of this subject can be found in Reference 2. The three most widely used separator materials in nickel-hydrogen cells are (1) high-quality remanufactured asbestos, (2) knit zirconium oxide cloth, and (3) nonwoven polyamide felts. They have been listed in increasing order of their average pore size. If an electrode expands by 10%, for example, the volume of electrolyte that as a first approximation is drawn into the swollen electrode is equal to the facial area of the electrode times the increase in thickness. For a typical plate used in a 3.5-inch diameter IPV cell, a 10% increase in its original 0.030-in thickness results in an increased electrolyte requirement of 0.361 cm^3. The electrode must expand against the Bellville washer and the compressive strength of the plastic gas screen. Reference 2 describes the calculation where the actual pore distributions of the components can be used to more accurately calculate the redistributed amounts of electrolyte between the cell components. When the electrolyte content in the separator is reduced to a critical value where diffusional limiting currents occur, cell failure caused by low end-of-discharge voltage is experienced. Separator material having a pore size distribution that results in a prolonged maintenance of adequate electrolyte levels will result in a longer cycle life.

The net effect of plate expansion is an increase in the void volume within a plate set. The electrolyte redistributes itself in a manner that equalizes the capillary pressure among all the communicating components. As a first approximation, the positive plate will tend to draw electrolyte from the separator due to the preponderance of its small pore character. A more exact solution must be based on knowing the pore size distribution of the three components making up the plate set.

2.2 Plaque Corrosion

Under the oxidizing conditions of the nickel electrode, the tiny particles making up the nickel sinter material can be very slowly oxidized according to Reaction (1).

$$Ni + H_2O \rightarrow Ni(OH)_2 + H_2\uparrow \quad (1)$$

During the charging step, the newly formed nickel hydroxide material can then be oxidized to the beta form or gamma form of nickel oxyhydroxide according to Reaction (2).

$$Ni(OH)_2 \rightarrow NiOOH + 0.5\ H_2\uparrow \quad (2)$$

This "added" active material does not have the cobalt content of the normal active material and is more difficult to charge and discharge due to its higher resistivity and greater tendency for oxygen evolution. Cells equipped with strain gauges or pressure transducers can closely monitor the added amount of hydrogen that results from these reactions. Reference 6 has several plots of pressure versus cycle life of nickel-hydrogen cells. Cycling data would suggest that electrodes made using the dry powder process have a greater tendency to corrode, whereas electrodes made using the slurry process are less prone to corrode. Modified manufacturing processes have resulted in techniques to passivate dry powder material in an attempt to reduce their rate of corrosion. Reference 6 also presents data on cycling cells with this newer plate material. By knowing the pressure rise and the internal volume of a cell design, the amount of hydrogen gas resulting from corrosion reactions can be calculated and related to the amount of nickel material that has been lost from the electrodes. It is to be noted from Reaction (1) that there is a twofold effect on the volumetric considerations that are brought about by the corrosion of the nickel sinter. First, a portion of the nickel sinter material is lost, and electrolyte would be drawn into the plate to replace the loss. However, the oxidation products become part of the electrode, and since the density of the active material is less than that of the nickel that is loss, there is a net loss of interior volume. Second, some of the water component of the electrolyte is lost as the water is consumed in Reaction (1).

The bounds of nickel corrosion can be estimated using a plot of end-of-charge pressure over the course of cycling a cell. The cells under study in Reference 6 were 48-plate Hughes cells using dry powder sinter plate material. Cells of this type had a beginning-of-life actual capacity of about 60 Ah to a 1.0-V cutoff. With a starting end-of-charge pressure of 600 psi, and using the perfect gas law, the interior free volume can be estimated to be 630 cm^3. The number of moles of hydrogen created to yield a pressure increase to 1100 psi would be about 0.876. Adding equations 1 and 2 would suggest that 34.3 g of nickel were lost over the 48 plates or 0.713 g per plate. A typical 0.030-in. powder plate starts with about 5.6 g of nickel sinter. In this example 13.4% of the nickel sinter material was corroded as the end-of-charge pressure increased from 600 psi to 1100 psi. Typical increases are much less than this.

The overall impact of plate corrosion results in a reduction in the porosity of the electrode since the newly formed nickel oxyhydroxide is less dense than the metallic nickel it replaces. The loss of water from the electrolyte results in a reduction in its volume along with an increase in the overall concentration of the remaining liquid.

2.3 Incorporation of KOH into the Gamma-Phase Lattice

The half cell potential for the formation of gamma-phase material is several tens of millivolts below that of the beta-phase material. Due to the slow kinetics of the former reaction, beta-phase material is the major constituent of the freshly recharged material. As beta-phase material is converted to gamma-phase material during overcharge or during the slow equilibration of the uncycled portion of charged active material, KOH is withdrawn from the electrolyte and incorporated into the lattice of the gamma phase. This lowers the electrolyte's concentration and, therefore, its conductivity. To a lesser extent, the electrolyte volume is reduced as well. During the subsequent discharge, some of the KOH is released back into the electrolyte. However, during the initial phases of the discharge, problems related to electrolyte conductivity can exist. This problem is exacerbated in cell designs that use minimal amounts of electrolyte, or low KOH concentrations, or where high concentrations of gamma phase material have accumulated. Under conditions discussed in Reference 10, the conductivity of the diluted KOH solution can be reduced to where it is insufficient to support high rates of discharge. This results in a condition known as diffusion-limiting current. Reaction (3) is intended to simulate this reaction.

$$3NiOOH + KOH + 2OH^- \rightarrow Ni_3O_6H{\bullet}KOH + H_2O + 2e^- \quad (3)$$

beta phase gamma phase

Adding this equation to the standard hydrogen evolution reaction equation;

$$2e^- + H_2O \rightarrow H_2 \uparrow + 2OH^- \quad (4)$$

resulting in the overall cell reaction leading to gamma-phase formation.

$$3NiOOH + KOH \rightarrow Ni_3O_6H{\bullet}KOH + H_2 \uparrow \quad (5)$$

A single 30-mil, 80% porous powder plate loaded with 1.65 g of nickel hydroxide per cm^3 of void volume contains about 4.75 g of active material. If all this material would be converted to the gamma phase, this would result in 51.25 millimole per plate. This would require one third of a mole per mole of KOH, or 17.08 millimole of KOH. Assuming a capacity of 1.5 Ah per plate (at 0°C to 0.0 V) and 3.5 g of 31% KOH per Ah, this quantity of electrolyte contains 29.06 millimole of KOH in the complete plate set (anode, separator, and cathode). More than half of the KOH would be consumed in the processes described in the above-listed equations. The electrolyte remaining would have an average KOH concentration of only about 15.6%. The electrolyte volume that started at 4.0 cm^3 per plate set would be reduced to 3.77 cm^3. The problem unfortunately is not that simple. The amount of gamma material formed is a function of the KOH concentration and the temperature. Reference 14 studied the gamma-phase phenomenon by measuring the cell capacity and cell pressure at the end of charge as a function of KOH concentration and temperature. Figure 1 plots cell capacities as a function of KOH concentration at 0°C as reported in this reference, along with data excerpted as noted from other sources. By assuming that a typical cell has a utilization of 108% when discharged at C/2 to a 1.0-V

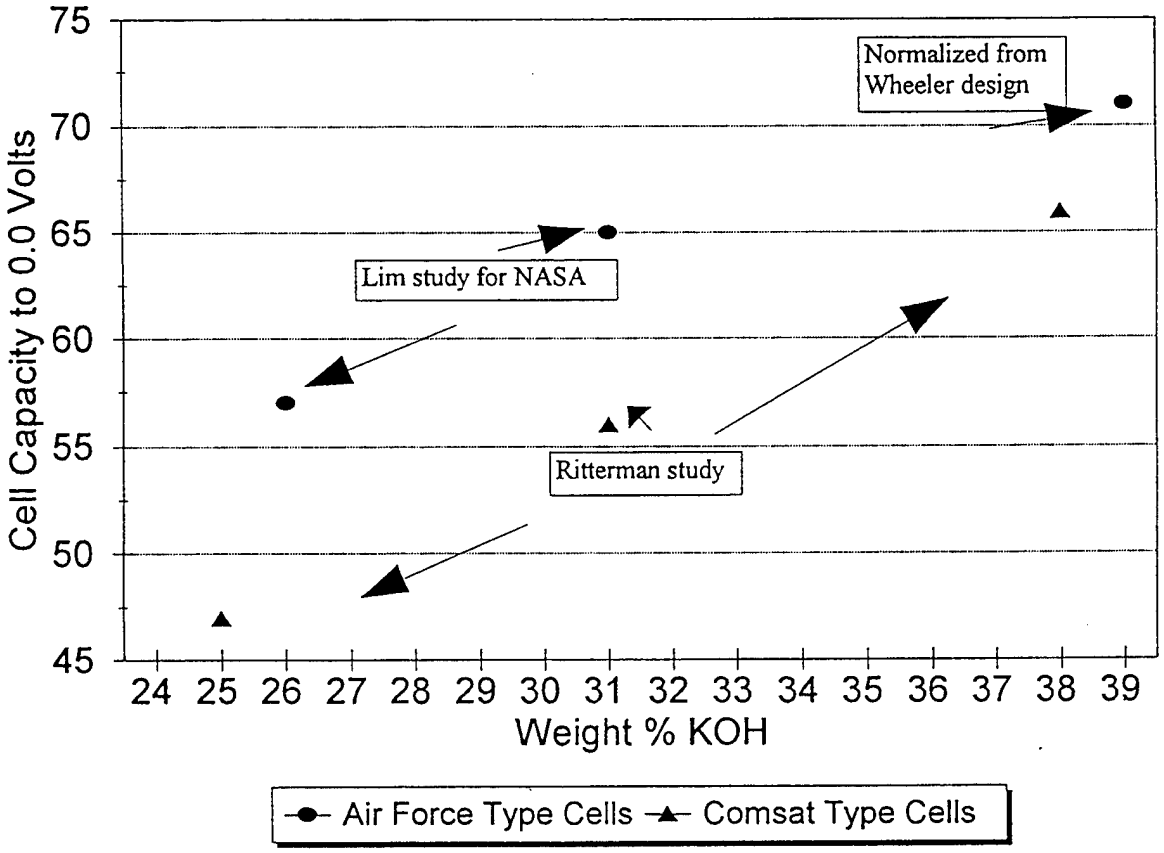

Figure 1. Cell capacity vs KOH concentration.

cutoff at 0°C in cells containing 31% KOH (using 10% as the residual capacity and 5% as the unavailable capacity), Figure 2 can be constructed. This study, as well as others, found that in flooded capacity tests, significantly higher amounts of capacity (higher levels of gamma phase) are obtained. This is caused by a smaller reduction in the KOH concentration as the plates are charged. In a fully sealed cell, with minimal amounts of electrolyte, the concentration changes from the discharged to the charged state are greater, and as the concentration is lowered as full charge is approached, the upper limit of gamma-phase material is reduced.

For this reason, it is almost impossible to convert all of the beta-phase material to the gamma phase under normal conditions within a completed cell. Estimates of this conversion can be made as follows. A cell's full capacity is often referenced following, for example, a 16-h charge at the C/10 rate at 0°C. Under these conditions, the manufacturer often states the percent utilization based on a one electron valence change of the total amount of active material within the cell. It is not unusual to reach a utilization value of 135% at 0°C in flooded capacity tests for moderately loaded plate material having desirable pore size distribution as typified by plaques made by the powder process. Studies on plate material have noted that at the C/2 discharge rate to a 1.0-V cutoff, about 10% more capacity remains (residual capacity) that can only be extracted at very low discharge rates, and another 5% is

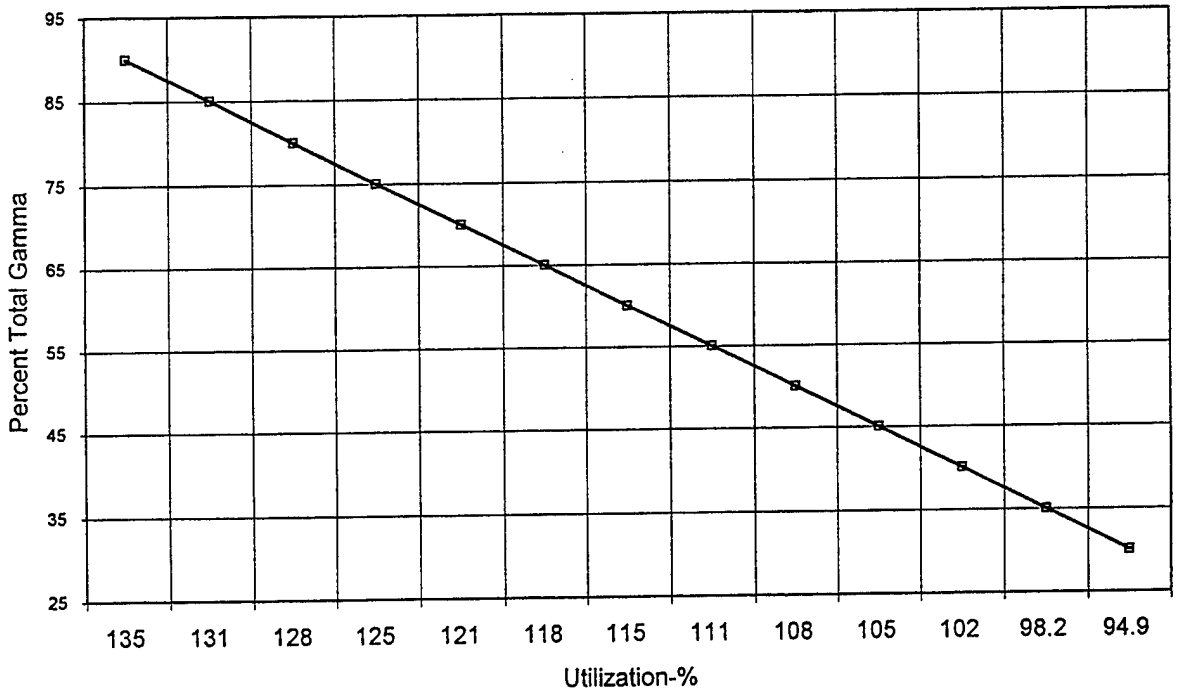

Figure 2. Percentage of gamma-phase material vs utilization of active material.

present (unavailable capacity) that can only be detected using wet chemical analyses of ground-up electrode samples. Assuming that the residual charge and the unavailable materials are converted to gamma-phase material, and the utilization of active material is 108% in a typical complete cell, it can be calculated that 50% (35% of this is available above 1.0 V) of the active material is converted under this set of charging conditions. ($0.35_{(\text{gamma phase})} \times 1.66$ electrons + $0.5_{(\text{beta phase})} \times 1.0$ electrons = 1.08.) During LEO cycling conditions where a complete cycle takes place every 90 min, it can be assumed that of the material being cycled, only a small fraction of that is converted to gamma-phase material. In GEO cycling, where extended periods of overcharge exist, percentages similar to those quoted during the characterization tests will be present. However, the uncycled material, including the residual and unavailable portions, will slowly be converted in part (as dictated by its equilibrium amount) to the gamma phase since this phase is thermodynamically more stable. Figure 3 shows the estimated distribution of material within nickel electrodes at different values of active material utilization.

As a further example relating to the impact of gamma-phase material on electrolyte volume and concentration, a cell being cycled under LEO conditions will be given. The cell is being cycled to 40% DOD in a LEO cycle, and only 10% of the material that is being repetitively cycled is assumed to be converted to the gamma phase. A typical value for the ratio of actual cell capacity to nameplate capacity is 1.2. This will be used in the calculation of the depth-of-discharge in the calculations for Table 1, which outlines the distribution of materials and phases. The table shows that incorporating KOH into the gamma phase results in significant reductions in the KOH concentration in the remaining electrolyte with only minor reductions in the volume of electrolyte. This undesirable conductivity

reduction in the electrolyte is reduced as the cell is discharged and the KOH is released back into the electrolyte.

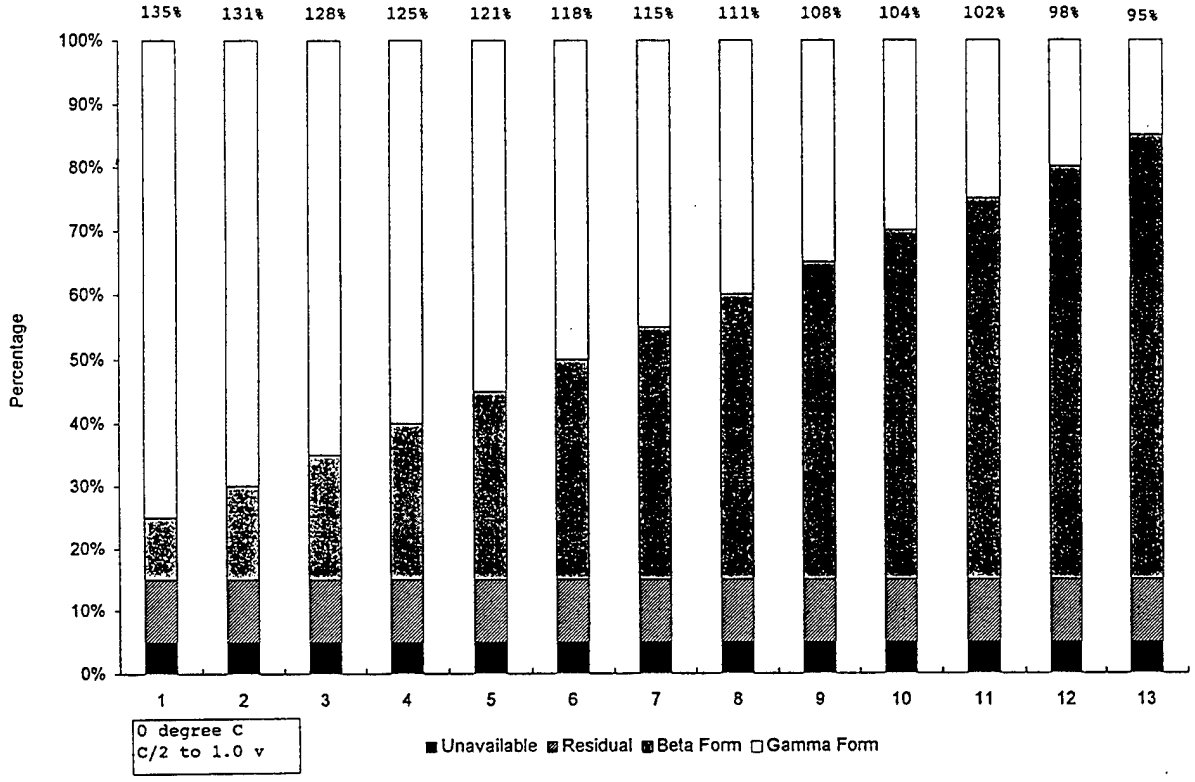

Figure 3. Distribution of active material for different utilizations.

Table 1. Impact of Gamma-Phase Material on a Cell Undergoing LEO Cycling to 40% DOD. (Nominal Composition: 31% KOH at full discharge)

Total material within the plate	51.25 mmole
Material assigned to unavailable (5%)	2.56 mmole
Material assigned to residual (10%)	5.12 mmole
Cycleable active material = 51.25 – (2.56 + 5.12)	43.57 mmole
At 40% DOD nameplate = 40/1.2	33.3% DOD actual
Material being cycled = 33.3% × 43.57	14.59 mmole
Amount converted to gamma during cycling	1.46 mmole
Amount cycled as beta	13.13 mmole
Amount of uncycled material = 51.25 – 13.13	38.12 mmole
Limit of gamma-phase conversion at 31% KOH	50%
Amount of uncycled material as gamma = 0.50 × 38.12	18.06 mmole
KOH required = 8.06/3	6.01 mmole
KOH available (as above)	29.06 mmole
KOH remaining = 29.06 – 6.01	23.05 mmole
KOH concentration at the end of charge	26.3%
Volume of 4.91 g of 26% KOH	3.90 cm^3
KOH released during discharge = 1.46/3	0.487 mmole
KOH concentration at the end of discharge	28.8%
Volume of 5.092 g of 29% KOH	3.95 cm^3
Initial volume of 5.25 g of 31% KOH was	4.04 cm^3
Percent volume loss at full charge	2.2%

2.4 Water Loss to Cold Cell Walls

For completeness, the loss of water from the plate pack to a colder cell wall will also be addressed. This is not a wearout mode as such, but a phenomenon that must be considered during the design phases of both the cell and the battery. Reference 10 addresses the topic of water loss from a warmer cell stack to an adjacent cooler cell stack under the driving forces of vapor-pressure gradients. Figure 4 plots the vapor pressure of different concentrations of KOH.

Certain thermal control arrangements in completed batteries permit coldplate surfaces to radiatively view the bottoms of cells. If there is a significant top-to-bottom temperature gradient within a cell that the coldplate is trying to control, it is possible for the coldplate to be cold enough to cause water to condense onto the colder surface of the cell bottom until there is an equilibration of the vapor pressures of the two different solutions. In Figure 4, horizontal lines connect solutions of equal vapor pressure. Reference 10 contains instructions for estimating the impact on electrolyte volumes due to this phenomenon. Reference 15 reports on studies carried out as a way of investigating and laboratory testing problems that were attributed to this phenomenon.

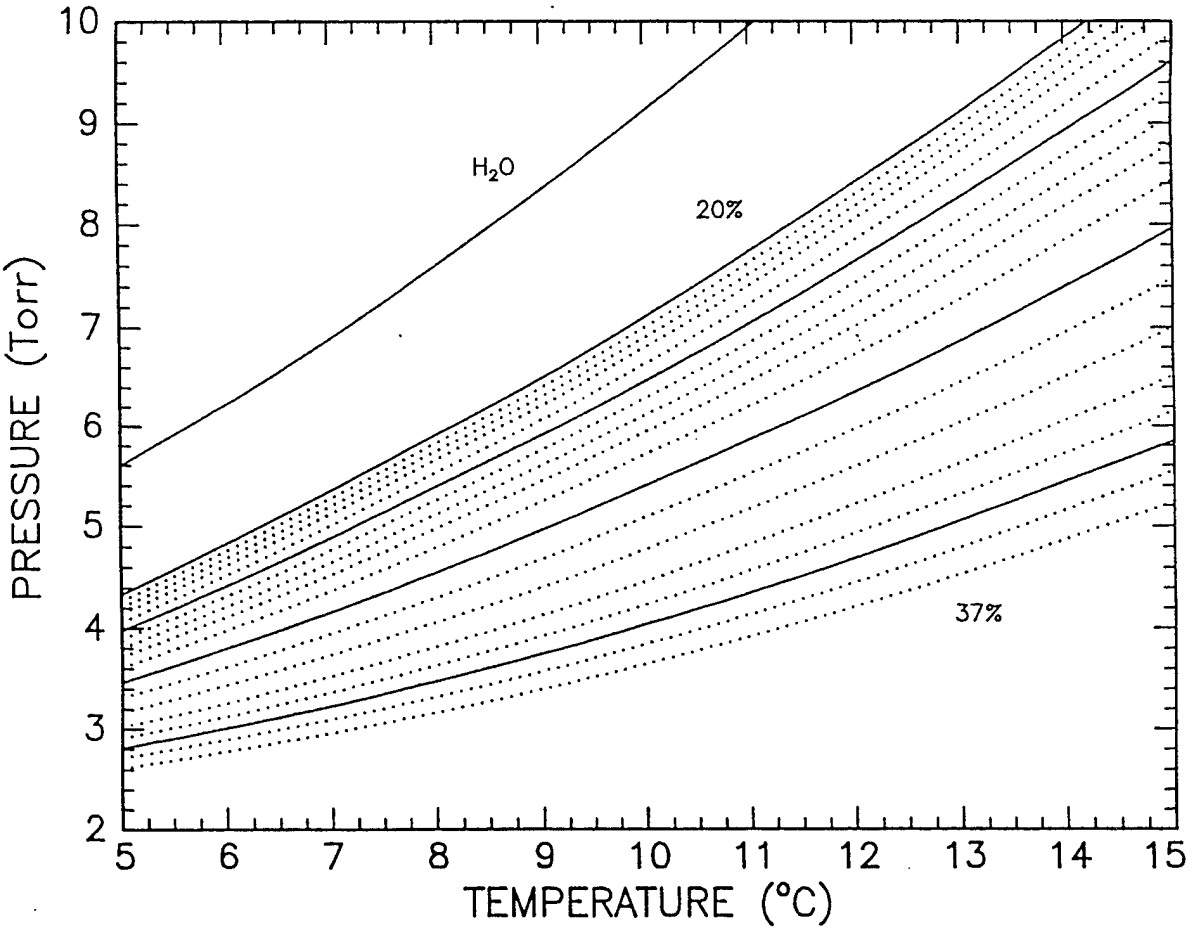

Figure 4. Vapor pressure of KOH solutions vs temperature.

By locating the condition of the plate pack (21% KOH in the previous example) on the chart at 10°C and solving the problem for a 5°C wall temperature, it can be shown that, at equilibrium, an unrealistic amount of water must be lost from the plate pack to the colder cell bottom. It can be concluded that other factors must be involved. Equilibrium conditions required equal vapor pressures. For an overall concentration of 22% in the plate pack, the first horizontal line that intersects the 5°C vertical occurs at a new plate pack concentration of 29%. The loss of volume in equilibrating the vapor pressures would reduce the electrolyte volume per plate pair from 3.8 cm^3 to 2.2 cm^3. The rate of return via wall wicking must exceed the rate of condensation onto the colder cell bottom. For this reason, this phenomenon will not be included as variable within the static cell model. A dynamic model that includes kinetics and mass transport features must be used for this situation.

3. Static Cell Model

The static model begins with determining the wettable void volumes of the hydrogen electrode, the separator, and the nickel electrode. In order not to violate any company proprietary information, only reasonable estimates or information that is readily available from the nickel-hydrogen cell literature will be used in the following examples. It is well known that there are many different combinations and permutations of cell components, but the methods used in working with the model will be the same.

The hydrogen electrode is based on fuel cell technology. A mixture of wettable catalyst powder and a hydrophobic Teflon emulsion are spread onto a current-carrying screen substrate and then sintered. The resultant electrode structure is made up of a mixture of hydrophobic gas channels and hydrophilic channels for the electrolyte. A hydrogen electrode will be assumed to be 0.006 in. thick and 50% porous. Of the total porosity, half is wettable, and the other half is nonwettable. The inner and outer diameters of the electrodes used in 3.5-inch IPV cells will be assumed to be 3.25 and 8.5 cm, respectively.

The most commonly used separators are (1) remanufactured, high-quality, fuel cell grade asbestos, (2) Zircar brand, knit zirconium dioxide cloth, or (3) nonwoven polyamide felt. Depending on the compressive forces applied by the Bellville washers that are typically used to spring load the plate pack, the different separators will have different degrees of compressibility and thickness/porosity when assembled into cells. Since the properties of Zircar cloth are widely known, and the use of asbestos is declining, single or double layer Zircar will be used in the examples to follow.

A wide variety of nickel electrodes can be used in these cells. The most common electrodes start with a fine-mesh nickel screen onto which small particles of nickel manufactured by the carbonyl process are sintered. At this point in the manufacturing process, the material is referred to as plaque. The plaques are then impregnated with nickel hydroxide by one of two widely used processes. By using an additive in the impregnation baths, the active material is doped with cobalt hydroxide as it is being formed. Typical combinations are as follows:

Plaque types	Dry powder: 80% porosity; slurry: 76% porosity
Loading levels	Grams of $Ni(OH)_2$ + additive per cm^3 of void volume: Low, 1.60 g/cm^3; Normal, 1.65 g/cm^3; High, 1.7 g/cm^3
Thicknesses	0.030 in. (0.76 mm), 0.035 in. (0.90 mm)
Cobalt levels	High (~10 weight %), Low (~5 weight %)

Once stacked together, compressed to the proper level, installed in its pressure vessel, and welded shut, electrolyte is added, and the cell is activated. Both the amount of electrolyte and the KOH concentration play critical roles in terms of the projected cycle life of the cell. It is at this point that the four factors that alter the electrolyte requirements of the cell come into play. At the same time, this is where the design features of the cell that are intended to counter the deleterious effects of these four factors reveal their effectiveness.

Several investigators have conducted studies on the minimum electrolyte requirements of alkaline cells. One employed a nickel-cadmium cell,[16] and the other[2] used components of a nickel-hydrogen cell. Figures 5 and 6 have been reproduced from their original works. Figure 5 shows that as the amount of electrolyte in a nickel-cadmium cell is reduced, there is a dramatic reduction in the pressure during overcharge as more cadmium surface becomes available for recombination. The electrochemical capacity, as measured by the minutes of discharge at the C/2 rate to the voltage cutoff, and the cell resistance are both very stable until an electrolyte content is reached where there is both a rapid increase in the cell resistance and a sharp drop in the usable capacity. Since the pore-size distribution in the individual cell components is such that the separator will tend to loose electrolyte to the finer pore sizes of the electrodes, a condition is reached within the separator where the current cannot be supported by the reduced electrolyte content. This is known as the diffusion-limiting current, and it results in a rapid increase in the internal impedance of the cell. This same type of phenomenon has also been noted in the work reported using only the components as employed in nickel-hydrogen cells. The procedure for these tests was as follows: (1) measured amounts of electrolyte were added to the components, (2) the components were pressed together as they would be in an actual cell, and (3) the electrolyte was allowed to redistribute itself to equilibrate the capillary forces within the three components. Following this, the resistance of the three-component stack was measured. Figure 6 shows that the experimental separator structures evaluated here were very sensitive to electrolyte content once they reached a lower critical value. Actual nickel-hydrogen cell data displaying this situation are very rare.

CELL: Ni-Cd BP's

WITH PP-PBI SEPARATOR WITH 274μ/SEPARATOR SPACING

C: CAPACITY

R: INTERNAL RESISTANCE

P: PRESSURE LEVEL AT C/10 RATE 64 HOUR CHARGE

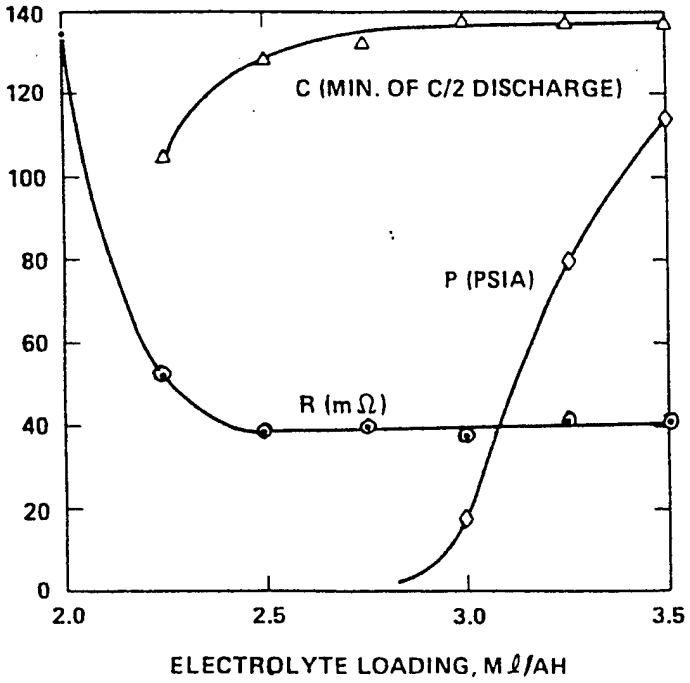

Figure 5. Typical cell parameters vs amount of electrolyte.

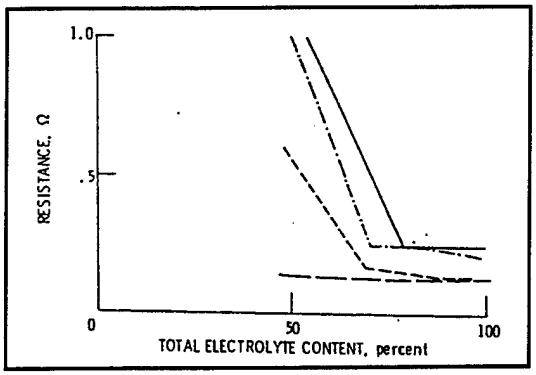

Figure 6. Resistance of cell components vs amount of electrolyte.

What is believed to be a case of cell dryout at a point when the electrodes were very new was reported in Reference 17. A cell was designed and optimized for high energy density. As such, there was a minimum amount of highly concentrated KOH added to the cells. The electrode structure was thought to be resistant to expansion, but it turned out not to be the case. The paper reported that the plates expanded about 12% at the point where there was a significant dropoff in capacity due to an early low voltage cutoff. Using electrolyte fill data that was made available and assuming that the expanding electrodes drew electrolyte out of the separator, it can be calculated that when the electrolyte content of Zircar separator dropped to only about 40% filled, it could not support a high rate (~C/2) discharge and still deliver full capacity. No mention was made of an unexpectedly low voltage during the first portion of the discharge as one would expect from a problem related to KOH being incorporated within the gamma phase. At the high concentration of KOH reported for these cells (39% KOH), they should not be subject to that type of problem.

4. Operation of the Model

The model requires a number of inputs to calculate the overall percentage of the cell's porous volume that is filled with electrolyte. Assuming that the separator will give up liquid to the positive electrode based on their relative pore sizes, the model also calculates the percentage of the separator pores that are filled with electrolyte. The inputs required are divided between (1) those that are directly measurable or known about the components, (2) those that are related to the cell, and (3) inputs that are projections of changes that might take place over the life of the cell. In the first group of inputs, the dimensions, porosities, densities, plate loading, etc. for each of the cell's components are required. The second group includes the features of the particular cell design. These are the amount of electrolyte, the concentration of electrolyte, the number of plate pairs, and number of layers of separator used in the cell. The third group of inputs includes the assumptions regarding the percentage of plate expansion, the percentage of plaque corrosion, and the percentage of active material that will be present in the gamma phase. This third group of inputs permits an estimate of effect of electrolyte distribution among the cell components for different assumptions related to the various cell degradation modes.

Reasonable assumptions are sometimes required for some of the required inputs. For example, the density values for the gamma and beta forms of charged active material are known to be different from the crystallographic textbook values. Plate expansion and plaque corrosion information, however, are available from literature sources or from analysis of cells that have completed life testing. Effective densities for the discharged form of beta $Ni(OH)_2$ can be estimated by assuming that a properly activated cell has very little free electrolyte, and that its pores are 100% filled. By selecting different densities for this material and knowing the amount of electrolyte added to the cell, a density value can be found that will yield a 100% fill for the overall cell. The textbook density for $Ni(OH)_2$ is listed as 4.14 g/cm^3, but battery-related literature[18] suggest 3.65 g/cm^3 as a more practical value.

The Appendix is a printout of the model using, as an example, the cell described in Reference 17. In the summary portion of this example, the impact of several assumed processes that are known to take place within a cell are noted.

5. Suggestions Related to Cell Design

By far the largest impact on the separator wetness is the expansion of the positive plates. When plaque material is corroded, the volume of water that is consumed is partially replaced by non-cobalt-containing active material, and when gamma-phase material replaces most of the beta material, its lower density partially makes up for the KOH loss. However, when positive plates expand, nothing is there to compensate for the newly formed wettable volume. A tightly compressed stack that is not free to expand is helpful if there is adequate strength in the plastic core that applies the compressive load to the stack. Under rare occasions, the plastic core has broken under the mechanical stress of the expanding stack. Extra electrolyte within the cell, either held in reserve within the separator or free electrolyte within the cell, is another method to counter the effect of cell dryout. Care must be taken that this extra electrolyte does not cause excessive popping, which can result in premature cell failure. A third method is to have a separator with a finer pore structure, such as asbestos, that can compete with the capillary forces of the positive electrode for electrolyte.

Another aspect of the cell that can be explored using this model is the impact of gamma-phase formation on electrolyte concentration. Cell designs that employ low KOH concentrations, coupled with minimal amounts of electrolyte, can suffer from the effects of low conductivity at high states of charge where the gamma-phase levels are highest. Again, based on a generic 62-plate pair stack, single-layer Zircar cell, starting with 100% electrolyte fill levels at different concentrations of KOH, Table 2 lists the minimum KOH concentrations when all of the possible conversion of beta-phase material to gamma-phase material has taken place. Figures 2 and 3 can be used to suggest limits of conversion to gamma-phase material, as evidenced by the variation of cell capacity as a function of KOH concentration.[14]

Table 2. Impact of Gamma-Phase Material on Electrolyte Concentration at Full Charge.

Initial % KOH	% Utilization	Grams Elect.	Initial % Filled	Final % KOH	Final % Filled
Single-Layer Zircar, 100% Initial Fill					
39	118	295	100	30	93.1
35	113	287	100	26	94.3
31	108	278	100	23	95.3
26	101	268	100	19	97.4
Double-Layer Zircar, 100% Initial Fill					
39	118	411	100	33	95.0
35	113	400	100	29	95.8
31	108	388	100	25	96.6
26	101	373	100	21	97.5

6. Conclusions

A static model for generic nickel-hydrogen IPV cells has been developed that helps explore the impacts of electrode expansion, electrode corrosion, and gamma-phase formation on the electrolyte concentration and its distribution between the different components within a cell. For GEO applications, the first discharge following an extended trickle charge can result in an abnormally high internal cell resistance during the initial portion of the discharge due to gamma-phase depletion of potassium hydroxide from the electrolyte. The potential advantages of using high concentrations of KOH for this application to gain the extra capacity due to the high gamma-phase content must be weighed against the excessive plate expansion that is possible if the plate strength is low.

In LEO applications where long cycle life is desired, provisions against early dryout of the separator must be made. Properly designed cells have been shown to be capable of cycle life in excess of 40,000 cycles at 60% DOD. These cells used only one layer of asbestos separator material. The pros and cons of single-layer separator systems as opposed to double-layer systems generally favor double-layer systems. This is felt to be a volume tolerance consideration as opposed to a requirement based on plate expansion and corrosion. The corrosion issue can be addressed using passivation techniques, and plate expansion can be addressed by requiring high levels of plate strength coupled with moderate loading levels and proper distribution of active material during impregnation.

References

1. Private communications

2. Abbey, K. M. and D. L Britton, "Pore Size Engineering Applied to the Design of Separators for Nickel-hydrogen Cells and Batteries," *Proceedings of the Eighteenth IECEC*; Orlando, FL, 1983.

3. Bernhardt, M. P. and D. W. Maurer, "Results of a Study on Rate of Thickening of Nickel Electrodes," *Proceedings of the Twenty Ninth Power Sources Symposium*, pp. 219–222, June 9–12, Cherry Hill, NJ, 1980.

4. Wheeler, J. R., "High Specific Energy, High Capacity Nickel-hydrogen Cell Design," *Proceedings of the Twenty Eighth IECEC*, Atlanta, GA, 1993.

5. Lim, H. S. and S. A. Verzwyvelt, "Nickel Electrode Expansion and the Effect of LiOH Additive," Vol. 1, pp. 104–108, *Proceedings of the Twentieth IECEC*, Miami Beach, FL, 1985.

6. Smithrick, J. J. and P. M. O'Donnell, "A Review of Nickel-hydrogen Battery Technology," Proceedings of the Thirtieth IECEC; Orlando, FL, 1995.

7. Lime H. S., G. R. Zelter, J. J. Smithrick, and S. W. Hall, "Destructive Physical Analysis Results of Nickel-hydrogen Cells Cycled In LEO Regime," Vol. 3, pp. 304–310, Twenty Sixth IECEC , Boston, MA, 1991.

8. Zimmerman, A. H. and P. K. Effa, Extended Abstracts of the Fall 1984 Meeting of the Electrochemical Society, Vol. 85-2, pp. 43–44, 1985.

9. Barnard, R., C. F. Randell and F. L. Tye, "Studies Concerning Charged Nickel Hydroxide Electrodes. I. Measurements of Reversible Potentials," *J. Appl. Electrochem.* Vol. 10, pp. 109–125, 1980.

10. Thaller, L. H. and A. H. Zimmerman, "Electrolyte Management Considerations in Modern Nickel-hydrogen and Nickel Cadmium Cell and Battery Designs," 1995 NASA Lewis Research Center SERT Conference.

11. Smithrick, J. J., M. A. Manzo, and O. G. Sanabria, "Advanced Designs for IPV Nickel-hydrogen Cells," *Proceedings of the Nineteenth IECEC*, San Francisco, CA, 1984.

12. Lime, H. S. and S. A. Verzwyvelt, "KOH Concentration Effect on the Cycle Life of Nickel-hydrogen Cells IV Results of Failure Analysis," *J. Power Sources*, Vol. 29, pp. 503–519, 1990.

13. Britton, D. L., "Characterization and Cycle Tests of Lightweight Nickel Electrodes," *Proceedings of the Symposium on Nickel Hydroxide Electrodes*, Edited by, D. A. Corrigan and A. H. Zimmerman, The Electrochemical Society, Vol. 90-4.

14. Ritterman, P. F., "Factors Affecting Nickel Oxide Electrode Capacity In Nickel-Hydrogen Cells," *Proceeding of the 1983 Goddard Space Flight Battery Workshop*, NASA Conf. Pub. 2331.

15. Earl, M., T. Burk and A. Dunnet, "Method of Rejuvenating Nickel-hydrogen Cells," *Proceedings of the Twenty Seventh IECEC*, Vol. 1, pp. 127–132 San Diego, CA, 1992

16. Verzwyvelt, S., "PBI Treated Polypropylene Battery Separator," The 1980 Goddard Space Flight Center Battery Workshop, Greenbelt MD.

17. Wheeler, J. R., "High Specific Energy, High Capacity Nickel-hydrogen Cell Design," *Proceedings of the Twenty Eighth IECEC*, Vol. 1, pp. 89–94, Atlanta, GA, Aug. 8–13, 1993.

18. Oshitani, M., K. Takashima, and Y. Matsumara, "Development of a High Energy Density Pasted Nickel Electrode," Proceedings of the Symposium on Nickel Hydroxide Electrodes, Edited by Corrigan, D. A. and Zimmerman, A. H., The Electrochemical Society, Volume 90-4.

Appendix—Generic Nickel-Hydrogen Static Cell Model

Positive Plate Information		Separator Information	
Outer Diameter-cm	8.4	Outer Diameter-cm	8.7
Inner Diameter-cm	3.2	Inner Diameter-cm	3.2
Thickness - .000-inches	0.036	Thickness - .000-inches	0.012
Plaque Porosity-%	82	Weight-gm	1.21
Denisty of Ni-gm/cc	8.9	Density-gm/cc	5.55
Plate Loading-gm/cc void	1.7	Number of Layers	1
Density of Ni(OH)2-gm/cc	3.97		
Density of NiOOH	4.56	Negative Electrode Information	
Density of Gamma Phase-gm/cc	3.71	Outer Diameter-cm	8.4
Percent of Maximum Gamma-%	60	Inner Diameter-cm	3.4
Percent Plate Expansion-%	5	Thickness -.000-inches	0.005
Percent Nickel Corrosion-%	5	Wet Porosity-%	25

Cell Information		Separator Calculations	
Weight of Electrolyte-gm	285	Gross Volume-cc	1.566
Number of Plates in Cell	62	Volume of zirconia-cc	0.218
Electrolyte Concentration-%	39	Separator Free Volume-cc	1.348
Nameplate Capacity-AHr	100	Total Separator Volume-cc	1.348

Estimates of Utilization/Gamma	
Maximum Utilization-%	118
Maximum Percent Gamma-%	65

Positive Plate Calculations		Negative Electrode Calculations	
New Cell		Gross Volume-cc	0.588
Gross Volume-cc	4.330	Free Volume-cc	0.147
Volume of Ni-cc	0.779		
Weight of Ni-gm	6.936		
Plaque Free Vol-cc	3.550		
Active Material as NiOOH-cc	1.324		
Free Volume of Plate-cc	2.227		
Plate Porosity-%	51.430		

New Cell Plate Set		Distribution of Electrolyte	
Total Free Volume-cc	3.722	Vol in Positive-cc	2.227
Electrolyte Volume/Plate-cc	3.307	Vol in in Negative-cc	0.147
Percent Filled-%(plate)	88.855	Vol Left for Separator-cc	0.933
Grams Electrolyte per AHr	2.850	Total in Plate Set-cc	3.307
		Separator Percent Filled-%	69.23
		Distribution of Electrolyte	
		Percent in Positive-%	67.34
		Percent in Negative-%	4.45
		Percent Left for Separator-%	28.22

Calculations for Gamma Phase	
Moles of Ni(OH)2/plate-mmole	65.110
Moles of KOH/plate-mmoles	31.956
Moles Gamma at EOC-mmmoles	25.322
KOH Required-mmoles	8.441
KOH Remaining-mmoles	23.515
New Percent KOH-%	31.995

Gamma Phase Plate Set		Distribution of Electrolyte	
New Electrolyte Volume-cc	3.124	Vol in Positive-cc	2.11
New Volume of Active-cc/plat	1.442	Vol in in Negative-cc	0.15
New Free Volume-cc/plate	2.109	Vol Left for Separator-cc	0.87
New Plate Set Free Volume-cc	3.604	Total in Plate Set-cc	3.124
Overall Percent Filled-%	86.678	Separator Percent Filled-%	64.384

		Distribution of Electrolyte	
		Percent in Positive-%	67.51
		Percent in Negative-%	4.707
		Percent Left for Separator-%	27.783
Calculations for Expanded Plates			
New Total Volume-cc	4.546		
Volume of Nickel-cc	0.779		
Weight of Nickel-gm	6.936		
Plaque Free Volume-cc	3.767		
Active Material Volume-cc	1.324		
Free Volume of Plate-cc	2.443		
Plate Porosity-%	53.743		
Expanded Plate Set		Distribution of Electrolyte	
Total Free Volume-cc	3.938	Vol in Positive-cc	2.443
Electrolyte Volume/Plate-cc	3.307	Vol in in Negative-cc	0.147
Percent Filled-%(plate)	83.970	Vol Left for Separator-cc	0.717
		Total in Plate Set-cc	3.307
		Separator Percent Filled-%	53.167
		Distribution of Electrolyte	
		Percent in Positive-%	73.882
		Percent in Negative-%	4.447
		Percent Left for Separator-%	21.672
Expanded and Gamma Plate Set		Distribution of Electrolyte	
Total Free Volume-cc	3.820	Vol in Positive-cc	2.325
New Electrolyte Volume-cc	3.124	Vol in Negative-cc	0.147
Percent Filled-%	81.766	Vol Left for Separator-cc	0.651
		Total in Plate Set-cc	3.124
		Separator Percent Filled-%	48.324
		Distribution of Electrolyte	
		Percent in Positive-%	74.440
		Percent in Negative-%	4.707
		Percent on Separator-%	20.853
Calculations for Corroded Plates			
Weight of Nickel Plaque-gm	6.936		
Weight of Corroded Ni-gm	0.420		
Weight of Remaining Ni-gm	6.516		
Weight Ni(OH)2 Corrosion-gm	0.664		
Weight of H2O Consumed-gm	0.258		
Total Water Lost-gm	15.970		
Water in Fresh Electrolyte-g	173.850		
KOH in Electrolyte-gm	111.150		
Water After Corrosion-gm	157.880		
Electrolyte Weight After-gm	269.030		
Concentration of Elect.-%	41.315		
Volume of Electrolyte-cc	190.376		
Weight of Elect./plate Set-g	4.339		
Volume of Elect/Plate Set-cc	3.071		
Corroded Plate Set		Distribution of Electrolyte	
Gross Volume of Ni Plate-cc	4.330	Vol in Positive-cc	2.128
Ni Volume after Corrosion-cc	0.732	Vol in in Negative-cc	0.147
NiOOH after Corrosion&Chg-cc	1.469	Vol Left for Separator-cc	0.795
Free Volume in Positive-cc	2.128	Total in Plate Set-cc	3.071
Free Volume in Negative-cc	0.147	Separator Percent Filled-%	58.980
Free Volume in Separator-cc	1.348	Distribution of Electrolyte	
Free Volume in Plate Set-cc	3.624	Percent in Positive-%	69.319
Electrolyte Per Plate Set-cc	3.071	Percent in Negative-%	4.789
Percent Filled-%(cell)	84.740	Percent Left for Separator-%	25.892

Expanded & Corroded Plate Set		Distribution of Electrolyte	
Expanded Gross Vol. Pos.-cc	4.546	Vol in Positive-cc	2.345
Ni Volume after Corrosion-cc	0.732	Vol in in Negative-cc	0.147
NiOOH after Corrosion-cc	1.469	Vol Left for Separator-cc	0.579
Free Volume in Positive-cc	2.345	Total in Plate Set-cc	3.071
Free Volume in Negative-cc	0.147	Separator Percent Filled-%	42.920
Free Volume in Separator-cc	1.348	Distribution of Electrolyte	
Free Volume in Plate Set-cc	3.840	Percent in Positive-%	76.369
Volume Electrolyte/plate-cc	3.071	Percent in Negative-%	4.789
Overall Percent Full-%	79.963	Percent Left for Separator-%	18.842
Corroded and Gamma Plate Set		Distribution of Electrolyte	
KOH in Electrolyte-gm	81.792	Vol in Positive-cc	2.011
Water Remaining-gm	157.880	Vol in Negative-cc	0.147
Electrolyte Concentration-%	34.127	Vol Left for Separator-cc	0.725
Volume of Electrolyte-cc	178.691	Total in Plate Set-cc	2.882
Volume of Elect./Plate Set-c	2.882	Separator Percent Filled-%	53.747
Overall Percent Full-%	82.215	Distribution of Electrolyte	
		Percent in Positive-%	69.760
		Percent in Negative-%	5.102
		Percent Left for Separator-%	25.138
Corr., Gamma, & Exp. Plate Set			
Expanded Gross Vol.Pos.-cc	4.428	Distribution of Electrolyte	
Volume of Elect./Plate Set-c	2.882	Vol in Positive-cc	2.227
Free Volume/Plate Set-cc	3.722	Vol in Negative-cc	0.147
Electrolyte Concentration-%	34.127	Vol Left for Separator-cc	0.508
Overall Percent Full-%	77.433	Total in Plate Set-cc	2.882
		Separator Percent Filled-%	37.687
Summary		Distribution of Electrolyte	
Case 1, New Cell		Percent in Positive-%	77.271
Overall Percent Filled	88.85	Percent in Negative-%	5.102
Separator Percent Filled	69.23	Percent Left for Separator-%	17.627
Electrolyte Concentration-%	39		
Case 2, Cell With Gamma Phase			
Overall Percent Filled	86.68		
Separator Percent Filled	64.38		
Electrolyte Concentration-%	32		
Case 3, Expanded Plates			
Overall Percent Filled	83.97		
Separator Percent Filled	53.17		
Electrolyte Concentration-%	39		
Case 4, Gamma and Expanded Plates			
Overall Percent Filled	81.77		
Separator Percent Filled	48.32		
Electrolyte Concentration-%	32		
Case 5, Corroded Plates			
Overall Percent Filled	84.74		
Separator Percent Filled	58.98		
Electrolyte Concentration-%	41		
Case 6, Corroded and Exanded Plates			
Overall Percent Filled	79.96		
Separator Percent Filled	42.92		
Electrolyte Concentration-%	41		
Case 7, Gamma and Corroded Plates			
Overall Percent Filled	82.21		
Separator Percent Filled	53.75		
Electrolyte Concentration-%	34		
Case 8, Gamma, Expanded, and Corroded Plates			
Overall Percent Filled	77.43		
Separator Percent Filled	37.69		
Electrolyte Concentration-%	34		

TECHNOLOGY OPERATIONS

The Aerospace Corporation functions as an "architect-engineer" for national security programs, specializing in advanced military space systems. The Corporation's Technology Operations supports the effective and timely development and operation of national security systems through scientific research and the application of advanced technology. Vital to the success of the Corporation is the technical staff's wide-ranging expertise and its ability to stay abreast of new technological developments and program support issues associated with rapidly evolving space systems. Contributing capabilities are provided by these individual Technology Centers:

Electronics Technology Center: Microelectronics, VLSI reliability, failure analysis, solid-state device physics, compound semiconductors, radiation effects, infrared and CCD detector devices, Micro-Electro-Mechanical Systems (MEMS), and data storage and display technologies; lasers and electro-optics, solid state laser design, micro-optics, optical communications, and fiber optic sensors; atomic frequency standards, applied laser spectroscopy, laser chemistry, atmospheric propagation and beam control, LIDAR/LADAR remote sensing; solar cell and array testing and evaluation, battery electrochemistry, battery testing and evaluation.

Mechanics and Materials Technology Center: Evaluation and characterization of new materials: metals, alloys, ceramics, polymers and composites; development and analysis of advanced materials processing and deposition techniques; nondestructive evaluation, component failure analysis and reliability; fracture mechanics and stress corrosion; analysis and evaluation of materials at cryogenic and elevated temperatures; launch vehicle fluid mechanics, heat transfer and flight dynamics; aerothermodynamics; chemical and electric propulsion; environmental chemistry; combustion processes; spacecraft structural mechanics, space environment effects on materials, hardening and vulnerability assessment; contamination, thermal and structural control; lubrication and surface phenomena; microengineering technology and microinstrument development.

Space and Environment Technology Center: Magnetospheric, auroral and cosmic ray physics, wave-particle interactions, magnetospheric plasma waves; atmospheric and ionospheric physics, density and composition of the upper atmosphere, remote sensing using atmospheric radiation; solar physics, infrared astronomy, infrared signature analysis; effects of solar activity, magnetic storms and nuclear explosions on the earth's atmosphere, ionosphere and magnetosphere; effects of electromagnetic and particulate radiations on space systems; space instrumentation; propellant chemistry, chemical dynamics, environmental chemistry, trace detection; atmospheric chemical reactions, atmospheric optics, light scattering, state-specific chemical reactions and radiative signatures of missile plumes, and sensor out-of-field-of-view rejection.